JACS
JOURNAL OF THE AMERICAN CHEMICAL SOCIETY

Communication

pubs.acs.org/JACS

Direct Simulation Evidence of Generation of Oxygen Vacancies at the Golden Cage Au_{16} and TiO_2 (110) Interface for CO Oxidation

Lei Li[†] and Xiao Cheng Zeng*[,†]

[†]Department of Chemistry, University of Nebraska-Lincoln, Lincoln, Nebraska 68588, United States

Supporting Information

ABSTRACT: We show Born–Oppenheimer molecular dynamics (BOMD) simulation evidence of the generation of oxygen vacancies at the golden cage Au_{16} and TiO_2 (110) interface for CO oxidation. Unlike the conventional Langmuir–Hinshelwood (L-H) mechanism, the CO molecule adsorbed at the perimeter Au sites of Au_{16} tends to attack a nearby lattice oxygen atom on the TiO_2 (110) surface rather than the neighboring co-adsorbed molecular O_2. Our large-scale BOMD simulation provides, to our knowledge, the first real-time demonstration of feasibility of the Mars–van Krevelen (M-vK) mechanism as evidenced by the generation of oxygen vacancies on the TiO_2 surface in the course of the CO oxidation. Furthermore, a comparative study of the CO oxidation at the golden cage Au_{18} and TiO_2 interface suggests that the L-H mechanism is more favorable than the M-vK mechanism due to higher structural robustness of the Au_{18} cage. It appears that the selection of either M-vK or L-H mechanism for the CO oxidation is dependent on the structural fluxionality of the Au cage clusters on the TiO_2 support.

Metal-oxide supported Au clusters can exhibit exceptionally high catalytic activity toward many reactions, such as CO oxidation,[1−5] water–gas shift reaction,[6,7] and hydrocarbons oxidation,[8,9] etc. CO oxidation in particular has been commonly used as a benchmark to characterize catalytic activity of gas-phase and metal-oxide supported Au clusters. Numerous mechanistic studies of CO oxidation on various gold cluster/TiO_2 (Au–TiO_2) systems have been reported in the literature.[9−15] However, mechanistic details of the high catalytic activity are still not completely understood.

One important issue has been the active oxygen species in CO oxidation process. Most experiments suggest that the adsorbed molecular oxygen at the Au–TiO_2 interface is most likely the active species for CO oxidation, whereas the surface lattice oxygen atoms are relatively inactive to the CO oxidation due to the lack of direct evidence of oxygen exchange between the TiO_2 and CO_2.[16−20] As such, the conventional Langmuir–Hirshelwood (L-H) mechanism has been widely invoked to describe the CO oxidation, whereas the Mars–van Krevelen (M-vK) mechanism is rarely considered. Recently Widmann et al. found that upon pre-oxidization of Au–TiO_2 systems, the atomic oxygen can act as an active species based on multiple gas pulse measurements in a temporal analysis of product (TAP) reactor.[21] Maeda et al. also observed enhancement of the conductance of Au–TiO_2 systems upon the formation of CO_2 and attributed the conductance enhancement to the generation of oxygen vacancies during CO oxidation.[22] Nevertheless, no direct evidence on the molecule level has been given to show the active role of the lattice oxygen atoms on the TiO_2 surface because of the challenge in *in situ* detection of oxygen vacancies during the CO oxidation. Here, we present the first Born–Oppenheimer molecular dynamics (BOMD) simulation evidence of the generation of oxygen vacancies in the course of CO oxidation. The BOMD trajectory allows us to visualize the formation of oxygen vacancies in real time during the reaction of CO with an adjacent lattice oxygen atom at the Au_{16}–TiO_2 interface, thereby confirming feasibility of the M-vK mechanism.

First, we perform a BOMD simulation of a soft-landing process of an Au_{16} cage cluster onto the TiO_2 (110) surface to obtain a more realistic TiO_2 (110) supported Au_{16} structure. The gas-phase Au_{16} cluster initially exhibits a highly symmetric hollow-cage structure.[23] The initial speed of the Au_{16} cluster is 200 m/s (~0.1 eV/atom). In the simulation, the rutile TiO_2 (110) surface is treated by a 6 × 3 TiO_2 (110) slab with 12 atomic layers, where the top 6 atomic layers are free to relax, while the bottom 6 atomic layers are fixed at their lattice position. The BOMD simulation is performed in the constant energy and volume (NVE) ensemble. Once a steady state of Au_{16}/TiO_2 structure is achieved from the soft-landing simulation, the final system is further optimized together with the co-adsorption of CO and O_2 molecules at the Au_{16}–TiO_2 interface. The fully relaxed system is then used for the reaction simulation with the temperature of the system controlled at ~125 K (in NVT ensemble). All the BOMD simulations are carried out using the CP2K software package.[24] Note that in the BOMD simulations, the effect of electron spin is not considered due to considerably higher computational demands for spin-polarized BOMD simulation. We did a test calculation based on three snapshot structures at time 0, 2, and 4 ps, using both spin-nonpolarized and -polarized calculations. We found that the spin-nonpolarized calculation yields consistent ground states (see Table S1) for the three important time steps as the spin-polarized calculation.

Snapshots of the soft-landing of Au_{16} cage on the TiO_2 (110) surface along with the corresponding pair distribution of the Au–Au and the Au–O distance as well as the coordination number analysis before and after the collision are shown in Figure 1. As seen in Figure 1a, the Au_{16} cluster starts to collide

Received: August 22, 2014
Published: October 22, 2014

dx.doi.org/10.1021/ja508666a | J. Am. Chem. Soc. 2014, 136, 15857−15860

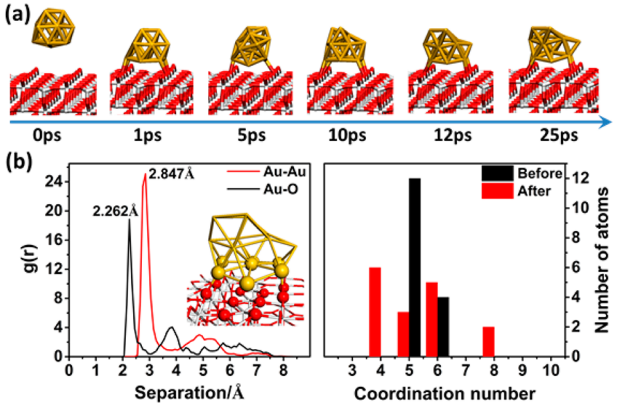

Figure 1. (a) Snapshots of a BOMD simulation of the soft-landing process for a hollow-cage Au_{16} onto TiO_2 (110) surface. The yellow, red, and white sticks represent gold, titanium, and oxygen atoms, respectively. (b) Pair distribution ($g(r)$) of the Au−Au and the Au−O distance (left panel). The first-layer Au atoms and the neighboring oxygen atoms on the TiO_2 (110) surface (highlighted in the inset image) are used for computing $g(r)$ of Au−O distance. The right panel illustrates the coordination number of Au atoms in hollow-cage Au_{16} prior to the collision (black bars) and after the collision from 10 to 25 ps (red bars).

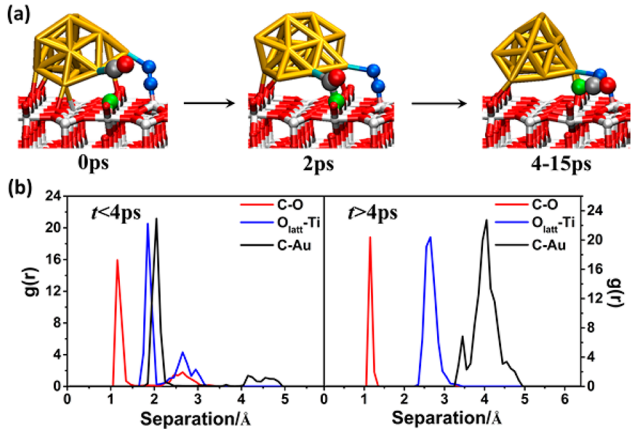

Figure 2. (a) Snapshots of BOMD simulation of CO oxidation at the Au_{16}−TiO_2 interface. The yellow, red, and white sticks represent gold, titanium, and oxygen atoms, respectively. The gray, red, green, and blue balls represent the carbon, oxygen (in CO), and lattice oxygen atoms and oxygen molecules, respectively. (b) The pair distribution of the C−O, C−Au, and O_{latt}−Ti distances before (t < 4 ps) and after (t > 4 ps) the formation of CO_2. The 'O' in the symbol "C−O" represents the oxygen (in red) from CO and the lattice oxygen (O_{latt}, in green). The "Ti" in the symbol "O_{latt}−Ti" represents the titanium atoms closest to O_{latt}.

with the TiO_2 (110) surface at ∼1 ps. During the collision, the Au_{16} structure deforms constantly, indicating the hollow-cage Au_{16} is more fluxional compared to the hollow-cage Au_{18} ($Au_{18\text{-cage}}$) which is a more robust Au cluster.[15] Upon structure relaxation for ∼10 ps, a relatively stable Au_{16} structure is obtained, for which the cage cluster can retain its structure with little deformation for ∼15 ps. During the collision, no structural fragmentation of Au_{16} is observed, as also indicated by the computed $g(r)$ of the Au−Au distance. Upon the collision, the Au_{16} cluster tends to attach to the TiO_2(110) surface due to the formation of Au−O bonds. As seen in Figure 1b, a sharp peak in the pair distribution ($g(r)$) of the Au−O distance is located at ∼2.262 Å, indicating formation of Au−O bonds at the Au_{16}−TiO_2 interface. The lack of any peak between the first and the second peak suggests no events of breaking Au−O bonds. Coordination number analysis indicates that the Au_{16} cluster apparently displays a different coordination environment after the soft-landing onto the TiO_2 surface due to structural deformation. The shrinkage of the hollow-cage structure leads to formation of highly coordinated Au atoms (i.e., 8-fold) and exposure of Au atoms with low-coordination (such as 4-fold), owing to the more fluxional structure of the Au_{16} cage.[25]

Next, the obtained Au_{16}−TiO_2 structure is used for the catalytic assessment. As shown in previous studies,[15,26,27] O_2 can strongly bind to low-coordinated Au atoms at the perimeter sites near the Au−TiO_2 interface, while CO can be adsorbed on the neighboring Au sites. Once the system is fully optimized, the BOMD simulation is carried out in the NVT ensemble at a relatively low temperature (T ∼125 K). The snapshots shown in Figure 2a and Supporting Movie S1 illustrate the time-dependent reaction process. Here, CO is oxidized by a lattice O atom (O_{latt}) rather than by the co-adsorbed O_2 molecule from the gas phase. In more detail, upon the adsorption of CO and O_2, the CO molecule tends to attack the O atom on a neighboring lattice site. The O−C−O_{latt} angle is enlarged to ∼180° with the C−O_{latt} distance reduced to ∼1.18 Å, indicating the formation of a CO_2 molecule. Meanwhile, the distance between O_{latt} and underneath Ti atoms is increased to ∼2.75 Å, demonstrating creation of an oxygen vacancy. To further confirm the formation of CO_2 and oxygen vacancy, the pair distribution ($g(r)$) of C−O, C−Au, and O−Ti distance is computed for two time intervals: before 4 ps (including the co-adsorption of CO and O_2 and the formation of CO_2) and between 4 and 15 ps (stability test of CO_2 at the oxygen vacancy). As shown in Figure 2b, during the formation of CO_2, there is a small peak at ∼2.7 Å, marking the initial distance between the C and the O_{latt}. Within the 4−15 ps, the small peak in $g(r)$ disappears, while a sharp peak at 1.18 Å arises. The disappearing and shifting of the small peak indicates the formation of C−O_{latt} bond with bond-length ∼1.18 Å. Similarly, the O_{latt}−Ti bond corresponds mainly to the length ∼1.85 Å before 4 ps, whereas the O_{latt}−Ti distance is enlarged to ∼2.75 Å after 4 ps, indicating the breaking of the O_{latt}−Ti bond and the formation of O vacancy. In summary, the sudden change of C−O and O_{latt}−Ti distance points out that the produced CO_2 is readily adsorbed on the oxygen vacancy, without dissociation of CO_2 and regeneration of O_{latt}.

The BOMD simulation of CO oxidation allows us to dynamically monitor how the charge fluctuates as a function of time for both Au_{16} cluster and CO during the CO oxidation (<4 ps). The Mulliken charge analysis for each structure can be obtained from the BOMD simulation. Indeed, such a charge analysis can well describe the charging/discharging process of Au clusters during the formation of CO_2, thereby recording the electron reservoir role of Au clusters in a dynamical manner rather than in static analysis of local structures as usually applied.[25] As shown in Figure 3, in the beginning, CO is positively charged due to the electron donation to positive Au atoms, and it can make an electrophilic attack to a neighboring negatively charged lattice O atom. During the electrophilic attack, CO starts to retrieve electrons from Au clusters, leading to charge reduction from CO but charge increase to Au cluster. At ∼1.9 ps, a structure with almost neutral CO is generated with ∼2.144 Å C−Au bond and 1.639 Å C−O_{latt} bond. The system is near the transition-state structure as indicated from

dx.doi.org/10.1021/ja508666a | J. Am. Chem. Soc. 2014, 136, 15857−15860

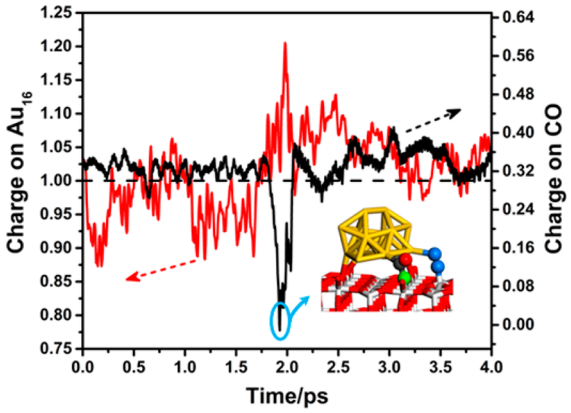

Figure 3. Mulliken charge analysis of the Au_{16} (red line) and CO (black line) during the formation of CO_2 in BOMD simulation of CO oxidation. Charge is in unit |e|. The inset image represents the structure where the OC−O_{latt} complex is formed. Identities of atoms are the same as those used in Figure 2a.

the reaction-pathway computation (Figure 4). Near the end of reaction, the charge state of Au_{16} is recovered. Hence, the Au

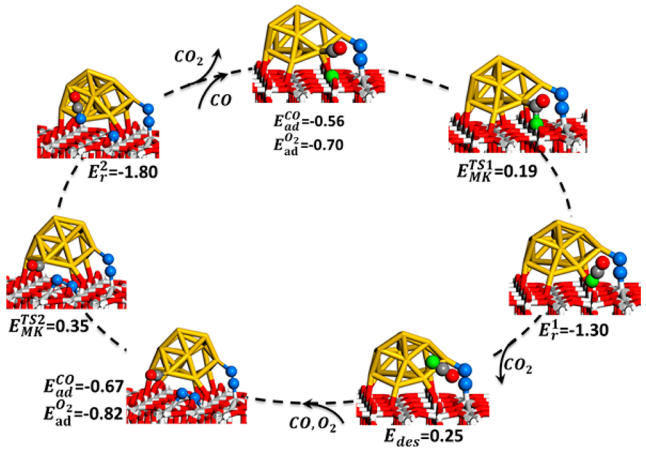

Figure 4. A schematic illustration of a full reaction pathway for CO oxidation at Au_{16}−TiO_2 interface, following the M-vK mechanism. E_{ad}^{CO}, $E_{ad}^{O_2}$, E_{des}, E_{MK}^{TS1}, E_{MK}^{TS2}, E_r^1, and E_r^2 represent the adsorption energy of CO and O_2, the desorption energy of CO_2, the reaction barriers for the generation and refilling of oxygen vacancy, and the corresponding reaction energies, respectively. The negative and the positive values indicate exothermic and endothermic process, respectively. Energy is in eV units. The identities of atoms are the same as those in Figure 2a.

cluster, as an electron reservoir, completes the charging/discharging process in one catalytic cycle, consistent with the previous static-charge analysis study.[25] In the charging/discharging process, the donation and withdraw of electrons are appreciable. For example, the highly charged Au clusters can easily draw electrons from CO, leading to strong CO binding. In this case, however, the CO attacking of either O_2 or the lattice oxygen atom is unable to facilitate the withdrawing of electrons from Au clusters, thus resulting in higher activation barriers. Indeed, the deactivating of a single Au atom is mainly due to this reason. On the contrary, the reduction of electronegativity of Au clusters may lead to weaker CO binding. Hence, it is important to seek a moderate charge state for the Au cluster to achieve higher catalytic activity. As an example, the formed Au−O−Ti^{4+} linkage reported by Green et al. can facilitate the charging/discharging process during the CO oxidation.[10]

To further confirm activity of lattice oxygen, we adopt a combined linear synchronous transit and quadratic synchronous transit (LST/QST) method, implemented in Dmol^3 7.0 package, to locate the transition state.[28,29] As shown in Figure 4, the computed reaction barrier (E_{MK}^{TS1}) for the generation of oxygen vacancy is as low as ∼0.19 eV (Figure 4), in good agreement with that (∼0.16 eV, Figure S1) obtained from the climbing nudged elastic band method (implemented in VASP 5.3 package).[30] This reaction barrier is much lower than that required through the L-H mechanism (∼0.63 eV, see Table 1

Table 1. O_2 Adsorption Energies and Reaction Barriers for CO Oxidation near Au_{16}−TiO_2 or $Au_{18\text{-cage}}$−TiO_2 Interface, Following Either M-vK or L-H Mechanism[a]

		M-vK mechanism		L-H mechanism	
	O_2 adsorption	E_{MK}^{TS1}	E_{MK}^{TS2}	E_{LH}^{TS1}	E_{LH}^{TS2}
Au_{16}	−0.70	0.19	0.35	0.62	0.31
$Au_{18\text{-cage}}$	−0.30	0.24	0.41	0.10	0.26

[a] E_{MK}^{TS1}, E_{MK}^{TS2}, E_{LH}^{TS1}, and E_{LH}^{TS2} represent the reaction barriers for the generation and refilling of oxygen vacancy in the M-vK mechanism, the formation of OCOO* intermediate, and the scission of O−O bond in the L-H mechanism, respectively. The energy is in eV units.

and energy profile reported in our previous paper, ref 15). In addition, the computed maximum reaction rate 1.5 × 10^7 s^{-1} (see Part II in Supporting Information(SI)) is much higher than that associated with previously reported L-H mechanism (2.1 × 10^2 s^{-1}).[15] Hence, the adsorbed CO molecule will most likely react with the lattice O atom rather than with the co-adsorbed O_2 molecule at the Au−TiO_2 interface, consistent with our BOMD simulation. The generated O vacancy can be refilled via dissociation of O_2 molecule with ∼0.35 eV activation barrier (E_{MK}^{TS2}, Figure 4). As a comparison, we also examine the M-vK mechanism at the Au_{16}−TiO_2 interface without a preadsorbed O_2. The reaction barriers are ∼0.25 and ∼0.34 eV for the generation and refilling of oxygen vacancy, respectively (Figure S2). The pre-adsorption of O_2 slightly lowers the barrier for the generation of oxygen vacancy. In summary, for the Au_{16}−TiO_2 system, the CO oxidation at the Au_{16}−TiO_2 interface favors the M-vK mechanism over the L-H mechanism.

To gain additional insights on the selection of M-vK and L-H mechanisms, we perform an independent reaction-pathway computation for the $Au_{18\text{-cage}}$−TiO_2 system based on both M-vK and L-H mechanisms.[15] As shown in Table 1, both the generation and the refilling of oxygen vacancy at the $Au_{18\text{-cage}}$−TiO_2 interface are required to overcome slightly higher reaction barriers (0.24 and 0.41 eV, respectively) than those required in Au_{16}/TiO_2 system (detailed illustration is given in Figure S3). Although the reaction barriers can still be overcome at modest temperature (e.g., 400 K), much lower reaction barriers are required through the alternative L-H mechanism, especially for the formation of the OCOO* intermediate (only 0.10 eV in energy barrier).[15] Moreover, as shown in Part II in SI, the CO oxidation via M-vK mechanism entails a much lower reaction rate than that via the L-H mechanism.[15] Therefore, unlike the Au_{16}−TiO_2 system, the co-adsorbed CO and O_2 at the $Au_{18\text{-cage}}$−TiO_2 interface tend to approach one another to form the OCOO* intermediate as observed in previous BOMD simulations.[15]

dx.doi.org/10.1021/ja508666a | J. Am. Chem. Soc. 2014, 136, 15857−15860

Our comparative studies suggest that the selection of either M-vK or L-H mechanism for the golden-cage/TiO_2 systems depends on fluxionality of the golden cage cluster and the binding strength of adsorbed O_2 molecule. Compared to the Au_{16} cage, the $Au_{18\text{-cage}}$ is much less fluxional. Not only does $Au_{18\text{-cage}}$ exhibit little structural deformation upon collision with TiO_2 surface but also does not budge upon co-adsorption of CO and O_2.[15] On the other hand, for the highly symmetric Au_{16} cage, either the collision or the adsorption of O_2 at the perimeter sites can induce notable structural deformation. In addition, the Au_{16} cage binds with O_2 more strongly than the Au_{18} cage, with an adsorption energy (−0.70 eV) which is about twice of that (−0.30 eV) for the $Au_{18\text{-cage}}$. Such a strong interaction with O_2 actually limits Au_{16}'s activity through L-H mechanism but can facilitate the M-vK mechanism.

In conclusion, we perform BOMD simulations to show direct reaction of CO with lattice oxygen atoms at the Au_{16}−TiO_2 interface and confirm the feasibility of the M-vK mechanism. An independent reaction-pathway search provides additional quantitative support of the likelihood of M-vK mechanism for the CO oxidation at the Au_{16}−TiO_2 interface. A comparative study with the more robust Au_{18} cage on TiO_2 indicates that the CO oxidation is more likely to follow the L-H mechanism rather than the M-vK mechanism, as the former entails a much lower energy barrier to form the OCOO* intermediate. We thus suggest that the M-vK mechanism is likely more favored for relatively fluxional Au clusters, whereas the L-H mechanism is more favored for robust Au clusters. Lastly, the dynamic trajectory of the BOMD simulation allows us to monitor the charge fluctuation of the system and the reservoir role of Au clusters, where the Au clusters can charge and discharge the CO molecule and facilitate formation of CO_2 molecule. This simulation study not only shows feasibility of the M-vK mechanism but also offers a better understanding of the selection of M-vK or L-H mechanism underlying exceptionally high activity of the Au−TiO_2 systems toward CO oxidation.

■ ASSOCIATED CONTENT

Supporting Information

A video of the trajectory of the BOMD simulation for simulating the CO oxidation on the Au_{16}−TiO_2 system; computed relative energies for three snapshot structures (at time 0, 2, and 4 ps); reaction-pathway searching for the generation of oxygen vacancy at the Au_{16}−TiO_2 interface based on climbing nudged elastic band method; schematic illustration of the CO oxidation via the M-vK mechanism in the Au_{16}−TiO_2 system (without O_2 co-adsorption) and the $Au_{18\text{-cage}}$−TiO_2 system (with O_2 co-adsorption); comparison of CO oxidation via M-vK and L-H mechanisms at the Au_{16}−TiO_2 interface; computed partial density of states (PDOS) of Au_{16} and $Au_{18\text{-cage}}$ clusters supported on the TiO_2 (110) surface; and detailed micro-kinetics analysis of the M-vK mechanism. This material is available free of charge via the Internet at http://pubs.acs.org.

■ AUTHOR INFORMATION

Corresponding Author

xzeng1@unl.edu

Notes

The authors declare no competing financial interest.

■ ACKNOWLEDGMENTS

This research is supported by grant from ARL (W911NF1020099) and by University of Nebraska Holland Computing Center.

■ REFERENCES

(1) Haruta, M.; Kobayashi, T.; Sano, H.; Yamada, N. *Chem. Lett.* **1987**, *16*, 405.
(2) Valden, M.; Lai, X.; Goodman, D. W. *Science* **1998**, *281*, 1647.
(3) Haruta, M.; Yamada, N.; Kobayashi, T.; Iijima, S. *Catal. Today* **1989**, *115*, 8.
(4) Xie, X. W.; Li, Y.; Liu, Z. Q.; Haruta, M.; Shen, W. J. *Nature* **2009**, *458*, 746.
(5) Fujikia, H.; Yamauchia, N.; Chijiiwaa, T.; Araia, S.; Tsubotab, S.; Haruta, M. *Catal. Today* **1997**, *36*, 9.
(6) Boccuzzi, F.; Chiorino, A.; Manzoli, M.; Andreeva, D.; Tabakova, T. *J. Catal.* **1999**, *188*, 176.
(7) Williams, W. D.; Shekhar, M.; Lee, W. S.; Kispersky, V.; Delgass, W. N.; Ribeiro, F. H.; Kim, S. M.; Stach, E. A.; Miller, J. T.; Allard, L. F. *J. Am. Chem. Soc.* **2010**, *132*, 14018.
(8) Haruta, M. *Catal. Today* **1997**, *36*, 153.
(9) Green, I. X.; Tang, W. J.; Neurock, M.; Yates, J. T. *J. Am. Chem. Soc.* **2012**, *134*, 13569.
(10) Green, I. X.; Tang, W. J.; Neurock, M.; Yates, J. T. *Science* **2011**, *333*, 736.
(11) Boccuzzi, F.; Chiorino, A.; Manzoli, M. *Mater. Sci. Eng., C* **2001**, *15*, 215.
(12) Bond, G. C.; Thompson, D. T. *Gold Bull.* **2000**, *33*, 41.
(13) Chen, M.; Cai, Y.; Yan, Z.; Goodman, D. W. *J. Am. Chem. Soc.* **2006**, *128*, 6341.
(14) Chen, M. S.; Goodman, D. W. *Science* **2004**, *306*, 252.
(15) Li, L.; Gao, Y.; Li, H.; Zhao, Y.; Pei, Y.; Chen, Z. F.; Zeng, X. C. *J. Am. Chem. Soc.* **2013**, *135*, 19336.
(16) Schumacher, B.; Denkwitz, Y.; Plzak, V.; Kinne, M.; Behm, R. J. *J. Catal.* **2004**, *224*, 449.
(17) Olea, M.; Tada, M.; Iwasawa, Y. *Top. Catal.* **2007**, *44*, 137.
(18) Olea, M.; Tada, M.; Iwasawa, Y. *J. Catal.* **2007**, *248*, 60.
(19) Liu, H.; Kozlov, A. I.; Kozlova, A. P.; Shido, T.; Asakura, K.; Iwasawa, Y. *J. Catal.* **1999**, *185*, 252.
(20) Olea, M.; Iwasawa, Y. *Appl. Catal., A* **2004**, *275*, 35.
(21) Widmann, D.; Behm, R. J. *Angew. Chem., Int. Ed.* **2011**, *50*, 10241.
(22) Maeda, Y.; Iizuka, Y.; Kohyama, M. *J. Am. Chem. Soc.* **2013**, *135*, 906.
(23) Bulusu, S.; Li, X.; Wang, L. S.; Zeng, X. C. *Proc. Natl. Acad. Sci. U.S.A.* **2006**, *103*, 8326.
(24) The CP2K developers group 2004.
(25) Wang, Y. G.; Yoon, Y.; Glezakou, V. A.; Li, J.; Rousseau, R. *J. Am. Chem. Soc.* **2013**, *135*, 10673.
(26) Gao, Y.; Shao, N.; Pei, Y.; Chen, Z. F.; Zeng, X. C. *ACS Nano* **2011**, *5*, 7818.
(27) Liu, C.; Tan, Y.; Lin, S.; Li, H.; Wu, X.; Li, L.; Pei, Y.; Zeng, X. C. *J. Am. Chem. Soc.* **2013**, *135*, 2583.
(28) Halgren, T. A.; Lipscomb, W. N. *Chem. Phys. Lett.* **1977**, *49*, 225.
(29) Peng, C.; Schlegel, H. B. *Isr. J. Chem.* **1993**, *33*, 449.
(30) Henkelman, G.; Uberuaga, B. P.; Jonsson, H. *J. Chem. Phys.* **2000**, *113*, 9901.